3-2015

Composition and Work Function Relationship in Os–Ru–W Ternary Alloys

Phillip D. Swartzentruber
University of Kentucky, pdswar2@uky.edu

Michael J. Detisch
University of Kentucky, michael.detisch@uky.edu

Thomas John Balk
University of Kentucky, john.balk@uky.edu

Composition and work function relationship in Os–Ru–W ternary alloys

Phillip D. Swartzentruber, Michael J. Detisch, and T. John Balk[a)]
Department of Chemical and Materials Engineering, University of Kentucky, 177 F. Paul Anderson Tower, Lexington, Kentucky 40506-0046

(Received 29 September 2014; accepted 23 December 2014; published 14 January 2015)

Os–Ru thin films with varying concentrations of W were sputter deposited in order to investigate their structure–property relationships. The films were analyzed with x-ray diffraction to investigate their crystal structures, and a Kelvin probe to investigate their work functions. An Os–Ru–W film with ~30 at. % W yielded a work function maximum of approximately 5.38 eV. These results align well with other studies that found work function minima from thermionic emission data on M-type cathodes with varying amounts of W in the coatings. Furthermore, the results are consistent with other work explaining energy-level alignment and charge transfer of molecules on metal oxides. This may shed light on the mechanism behind the "anomalous effect" first reported by Zalm *et al.*, whereby a high work function coating results in a low work function for emitting cathode surfaces. An important implication of this work is the potential for the Kelvin probe to evaluate the effectiveness of dispenser cathode coatings. © *2015 American Vacuum Society*.
[http://dx.doi.org/10.1116/1.4905499]

I. INTRODUCTION

Os–Ru thin films are typically used as coatings for dispenser cathodes. A dispenser cathode is an electron-emitting device used to generate a stream of electrons. Heating the dispenser cathode to a sufficiently high temperature allows for electrons within the cathode to gain enough energy to overcome the potential energy barrier and move into the vacuum. A dispenser cathode usually consists of a porous tungsten (W) pellet that contains a barium–calcium–aluminate ($xBa–yCa–z(Al_2O_3)$) compound within the pores. Heating the cathode allows for Ba to traverse to and adsorb onto the surface. It is well known that the adsorption of Ba on the surface allows cathodes to emit electrons at a much lower temperature than, for example, bare W. However, at high temperature, Ba does not remain on the cathode surface permanently and readily evaporates into the vacuum. Once the Ba is lost from the surface, the temperature of the cathode must be raised significantly in order to maintain the current density of emitted electrons. Therefore, it is important for Ba to be resupplied to the surface and the material impregnated in the pores acts to do just that.

It was discovered by Zalm *et al.*[1] that applying a coating of osmium (Os) to a cathode resulted in thermionic emission at temperatures significantly lower than uncoated cathodes. Surprisingly, even though this enhances electron emission, the work function of Os is not lower than that of W. In fact, the work function is significantly higher, with reports of up to 5.7 eV (Refs. 1–3) as opposed to 4.6 eV for W. Zalm termed this phenomenon the "anomalous effect," through which a high work function coating results in a lower work function for an emitting cathode. An osmium–ruthenium (Os–Ru) alloy coating with performance comparable to Os coatings was eventually adopted to mitigate safety concerns over working with pure Os. The Os–Ru coated, often termed M-type, dispenser cathodes are well known throughout the dispenser cathode industry for their marked improvement in electron emission over bare (B-type) dispenser cathodes.[1] The ability to operate dispenser cathodes at lower temperatures allows their lifetime to be extended due to lower Ba evaporation rates and a reduction in degradation of the Os–Ru film that results from the interdiffusion of W and Os–Ru.

In order for a dispenser cathode to reach suitable current density levels, the Ba from the impregnate compound must first diffuse to and cover the surface. When Ba has covered the surface of the cathode, the cathode is said to be activated. The activation process involves heating the cathode to high temperatures (1250 °C) until a sufficient current can be drawn. Over the course of the activation process and especially during operation, W from the substrate will diffuse into the Os–Ru coating.[4–7] The result is a ternary alloy of W, Os, and Ru that interacts with Ba, rather than just the initial Os–Ru coating. Some researchers have postulated that the Os–Ru–W alloy, rather than simply the Os–Ru coating, is responsible for the notable emission enhancement.[4] Additionally, others[7] believe that if too much W is incorporated, the emission enhancement from the coating disappears. Thomas and Gibson[8] have studied the work function variation versus alloy concentration for W–Ir and W–Re alloys. They used current density measurements to determine the work function of W–Ir and W–Re alloys as a function of composition. They found that a work function minimum occurred near 40 at. % W in the W–Ir films deposited on standard B-type cathodes. For W–Re, a minimum occurred near 50 at. % W, but the cathode was a controlled porosity cathode and not a standard B-type cathode. They were also able to extract similar data from the works of Brion *et al.*[9] and Shih *et al.*[10] on W–Os alloys that agreed reasonably well with their data.

In this work, thin films of Os–Ru–W with a range of compositions were deposited to explore trends in work function and crystal structure with composition. The roles of W, Os–Ru, and Ba on the superior emission characteristics of

[a)]Electronic mail: john.balk@uky.edu

M-type cathodes will be interpreted from the work function and crystallographic information.

II. EXPERIMENT

In order to create Os–Ru–W films with a range of W concentrations, a DC magnetron sputtering system (ATC Orion by AJA International Inc.) was used. The sputtering system had a base pressure of less than 1×10^{-5} Pa (7.5×10^{-8} Torr). The films were sputter deposited on a molybdenum–rhenium (Mo–Re) substrate that had been laser-cut into 5 mm × 10 mm pieces, as well as onto porous W pellets. The pieces of Mo–Re and the porous W pellets were mounted linearly across a substrate carrier so that once transferred into the DC magnetron sputtering system, the lines of substrate materials could be aligned parallel to and centered between two targets, Os–Ru and W (or Ir and W). By holding the substrate carrier in a fixed (nonrotating) position during sputtering, this configuration allowed for a natural composition gradient to develop along the pieces during deposition, e.g., with one end rich in Os–Ru and the other end rich in W. The slope of the composition gradient was controlled by adjusting the voltage applied to the targets. The Os–Ru target was composed of nominally 80 at. % Os and 20 at. % Ru, while the W and Ir targets were 99.99% pure. Before film deposition, the substrates were sputter cleaned with argon (Ar) plasma using RF substrate biasing (252 V forward DC) for 90 s at 3.33 Pa (25 mTorr). A gradient rich in Os–Ru was prepared by sputtering Os–Ru at 393 V DC (110 W) and W at 316 V DC (50 W) with Ar ions for 6 min and 40 s at 2.5 mTorr. The film was nominally 100 nm thick. A W-rich gradient was prepared by sputtering Os–Ru at 347 V DC (34 W) and W at 354 V (162 W).

The composition gradient was determined using x-ray energy-dispersive spectroscopy (EDS) and x-ray photoelectron spectroscopy (XPS). EDS was carried out in a Hitachi S-3200-N scanning electron microscope equipped with an Evex-EDS system. A Thermo Scientific K-Alpha XPS was used to determine the composition at the surface of the samples. After ion etching with Ar to remove surface contamination, a 400 μm wide beam of monochromatic aluminum K-alpha x-rays was used to irradiate the sample in the XPS. The crystal structure variation along the composition gradient was determined with x-ray diffraction (XRD) in a θ–2θ configuration on a Siemens D500 Krystalloflex Diffractometer. Samples were scanned from 30° to 90° (2θ) in 0.01° steps at 0.5°/min.

The work function variation along the composition gradient was determined using a Kelvin probe (KP Technology), which utilizes the contact potential difference (CPD) between the sample and a vibrating head to determine the work function. The contact potential difference arises as a result of the difference in work function between the sample and tip. If the work function of the tip is well defined, the measured contact potential difference can be used to calculate the work function of the sample

$$\Phi_{\text{sample}} = \Phi_{\text{tip}} + eV_{\text{CPD}}, \quad (1)$$

where Φ_{sample} is the work function of the sample, Φ_{tip} is the work function of the tip, and V_{CPD} is the contact potential difference. The Kelvin probe used here was mounted in a UHV chamber evacuated to a pressure of better than 6.67×10^{-6} Pa (5×10^{-8} Torr) and is shown in Fig. 1.

The absolute work function of the tip was determined using photoemission and a UV LED light source so that the measured CPD values could be used to determine specimen work functions according to Eq. (1). The CPD was measured at least 500 times for each sample while under vacuum in order to obtain an accurate average and standard deviation. This technique results in an averaged measurement of work function with associated error under 10 meV for an individual sample. Comparing multiple analyses at different times for a single sample, the variation in measured work function was less than 50 meV, which is therefore taken to be the maximum error.

III. RESULTS

A. Composition and Crystal Structure

The codeposition of W and Os–Ru resulted in a gradient in composition ranging from 8 to 95 at. % W, as measured by XPS and detailed in Fig. 2. The gradient in composition with respect to distance appeared more sigmoidal than linear. More importantly, however, is that the gradient was smooth with no discontinuities, as this avoided large gaps in composition.

XRD scans for a select number of compositions are shown in Fig. 3. The interaction depth of x-rays used for XRD is on the order of 10 μm. Considering that the films studied here are more than an order of magnitude thinner than the interaction depth, diffraction from the substrate will likely be detected and the diffracted intensity will likely be greater than that from the film alone. This was indeed the case, as all diffraction scans exhibited four peaks that appeared at the same angles for all samples, and these were attributed to the BCC Mo–Re substrate. Calculations based

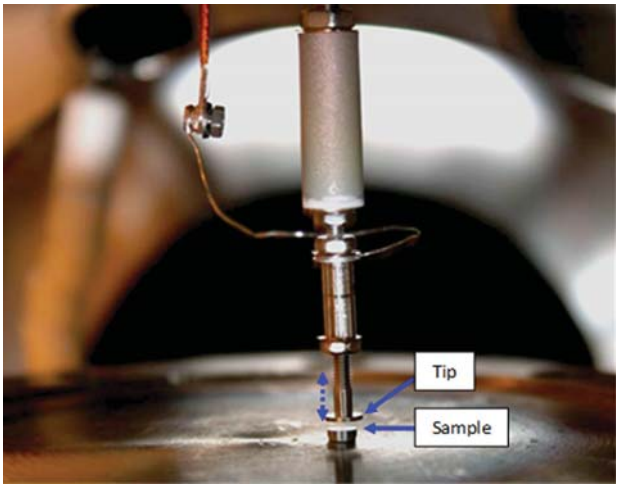

FIG. 1. (Color online) UHV Kelvin probe showing the tip and sample configuration. The probe tip vibrates vertically above the sample. The sample must be grounded with respect to the tip and remain free of any vibration.

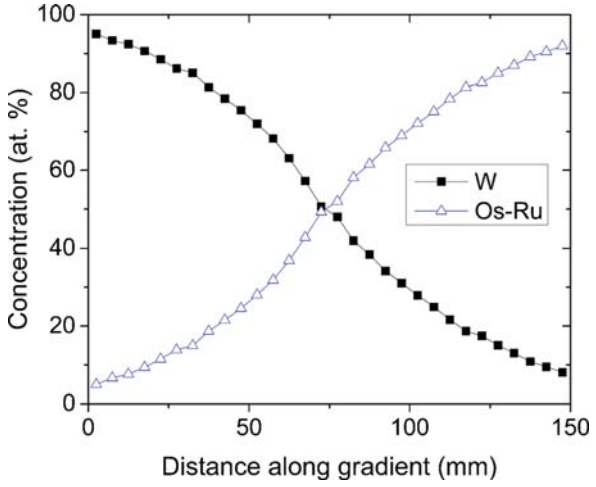

FIG. 2. (Color online) Concentration gradient of W–Os–Ru ternary alloy films deposited on Mo–Re and porous W substrates. The composition for every sample was determined using XPS and select samples were measured with EDS as a cross-check, which gave similar compositions.

on the lattice parameter for BCC Mo–Re ($a = 3.12$ Å, as determined from a separate XRD scan of the substrate material) predicted peak positions that matched those detected in the scans of coated samples. Furthermore, calculation of the theoretical relative intensities of the peaks matched well with the observed relative intensities of those peaks. This was especially important in order to avoid attributing the smaller peak near 90° (2θ) to any of the films, since the intensities were on the same order of magnitude. With the substrate peaks accounted for, the remaining peaks were attributed to the films.

XRD scans of the Os–Ru target material confirmed the hexagonal close-packed (HCP) crystal structure with lattice parameters of $a = 2.72 \pm 0.04$ Å and $c = 4.30 \pm 0.06$ Å, yielding a c/a ratio of 1.58 ± 0.05. These parameters agree well with the literature values for pure Os and Ru, both of which are HCP metals. The error for each lattice parameter was determined by taking the derivative of Bragg's Law and calculating the error in lattice plane spacing for each indexed diffraction peak, based on the uncertainty in peak location. The uncertainty in peak location was taken to be one-half of the step size used for XRD scans. The uncertainty stated above for the c/a ratio (± 0.05) was determined from the largest and smallest ratios based on uncertainties in the lattice parameters. This may be an overestimate of c/a error. As shown in Fig. 4, a c/a error of ± 0.05 is as large as the figure scale for this ratio. Nonetheless, a clear trend in c/a ratio with W content is observed.

For dilute concentrations of W, the alloy was assumed to have an HCP crystal structure with lattice parameters near that of the bulk Os–Ru alloy. The peaks from the W–Os–Ru film with 8 at. % W corresponded to the peak pattern of an HCP crystal. Furthermore, the lattice parameters measured for this alloy film were $a = 2.73 \pm 0.04$ Å and $c = 4.32 \pm 0.06$ Å, yielding a c/a ratio of 1.59 ± 0.05. These values are similar to those of bulk Os–Ru, corroborating the existence of an HCP structure for the alloy film. W has a larger atomic radius than both Os and Ru and it should be expected that alloying with

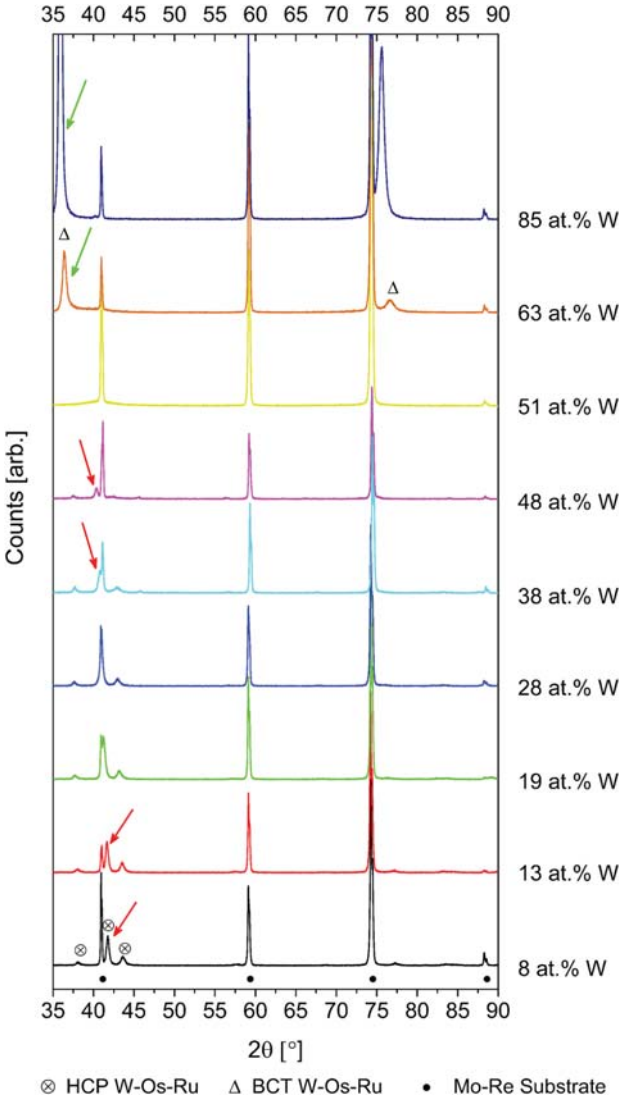

FIG. 3. (Color online) XRD scans of W–Os–Ru ternary alloys indicating a shift in the HCP peak position with increasing W concentration (starting from the bottom, peaks indicated by arrows) and showing the formation of a BCT phase (arrows above the top two XRD scans).

W would result in an increase in unit cell volume, assuming a substitutional solid solution. This was evidenced by a shift in the 2θ position in the XRD scans of the W–Os–Ru alloys. The (0002) peak (indicated by red arrows when distinguishable from the substrate peak) shifts to lower diffraction angles as the concentration of W increases. The (10–11) peak experiences similar shifts, while the (10–10) peak shifts only slightly. It is not surprising that the (0002) and (10–11) peaks shift in a similar manner because the (10–11) interplanar spacing is related to the magnitude of the c lattice parameter. However, it is somewhat surprising that there was very little shift in the (10–10) peak position, indicating that the unit cell dimensions increased primarily along the c-axis for films with higher concentrations of W.

The W–Os–Ru ternary alloys in this study appear to form a continuous, substitutional solid solution, for W content below 50 at. %. For an idealized HCP structure, consisting

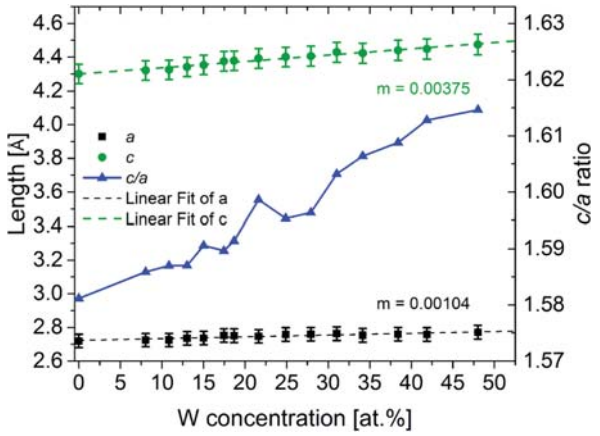

FIG. 4. (Color online) Comparison of variations in c and a lattice parameters with W concentration. The variation in c/a ratio is also shown plotted against the right axis. The c lattice parameter increases over 3.5 times faster than the a lattice parameter, indicating that the unit cell expands primarily along the c axis as W is added to the HCP Os–Ru phase.

of rigid perfect spheres that contact each other in a close-packed arrangement, a c/a ratio of 1.633 would be expected. However, the W–Os–Ru alloys characterized here do not exhibit this ratio. As discussed above and also presented in Fig. 4, the c/a ratio rises from 1.58 (Os–Ru without any W) to more than 1.61 (50 at. % W in the ternary alloy). While one could interpret this trend as elongation of the unit cell along the c-axis at higher concentrations of W, it is perhaps more appropriate to view this as the c/a ratio approaching the ideal value of 1.633 at higher concentrations of W. For the binary Os–Ru alloy, the low c/a ratio suggests that the effective shape of the atoms is slightly ellipsoidal or oblate spheroidal, rather than perfectly spherical. As the W concentration increases (up to 50 at. %) in the alloy film samples, the rising c/a ratio would indicate that the average atomic shape becomes more spherical. Figure 4 shows that the a lattice parameter remains relatively constant over the range of W concentrations, while the c lattice parameter increases (as does the c/a ratio, plotted against the right ordinate). If the average atomic shape in binary Os–Ru is ellipsoidal, then the long axis would be oriented parallel to the basal plane. With increasing W concentration in the alloy, the ellipsoidal shape expands more along its short axis than the long axis, resulting in a more spherical atomic shape. The effective atom shape is a result of the bonding between alloying elements, and the bond configuration appears to be modified by increasing W concentration.

A phase transformation to the body-centered tetragonal (BCT) structure occurs near 50–60 at. % W and agrees well with a similar transformation seen in W–Os alloys. According to the W–Os phase diagram,[11] W–Os undergoes a phase transformation from HCP to a BCT σ-phase at 65 at. % W. Because the system investigated here was a ternary alloy of W–Os–Ru, rather than a binary alloy of W–Os, it was not known whether a similar transformation should occur. This was considered during analysis of the new peaks that appeared in XRD scans of ternary alloys with more than 60 at. % W (see Fig. 3). If a BCT crystal structure is assumed for a substitutional solid solution of W, Os, and Ru atoms, and if the lattice parameters are assumed equal to those of the W–Os σ-phase ($a = 9.66$ Å, $c = 5.01$ Å as reported by Green *et al.*[4]), then the new peaks correspond to the (002) and (004) planes of the BCT phase. Therefore, it appears that the W–Os–Ru ternary alloys in this study crystallize in the HCP structure for W concentrations below 50 at. % and in the BCT structure for W concentrations above 60 at. %, similar to what is observed in the W–Os system.

It is interesting to note that at lower W compositions (e.g., 51 at. % W), there is an absence of diffracted x-ray intensity from the film. It is unclear why this happened but it may be that the film was either amorphous or the grains had a combination of low symmetry and/or unfavorable orientation for diffraction. In any case, it is clear that the crystal structure differs for high and low concentrations of W. Another interesting note is that for the alloy films with a BCT structure, the intensities of diffraction peaks were significantly greater than for the films with an HCP structure. This could be attributed to a strong {001} texture in the BCT films, as only the (002) and the higher order (004) reflections were observed.

B. Work Function

The work function exhibits a dependence on W concentration, as shown in Fig. 5. A 3 part piece-wise linear fitting function was used to fit the data in Fig. 5. As the W concentration increases to 30 at. % W, the work function also increases to a value of 5.38 eV. However, above 30 at. % W the work function generally decreases as the W concentration increases to 95 at. %. This composition where work function exhibits its maximum corresponds closely to the W concentration measured in M-type cathodes during operation.[6,8,10,12–15] Furthermore, the hypothesis that a high work

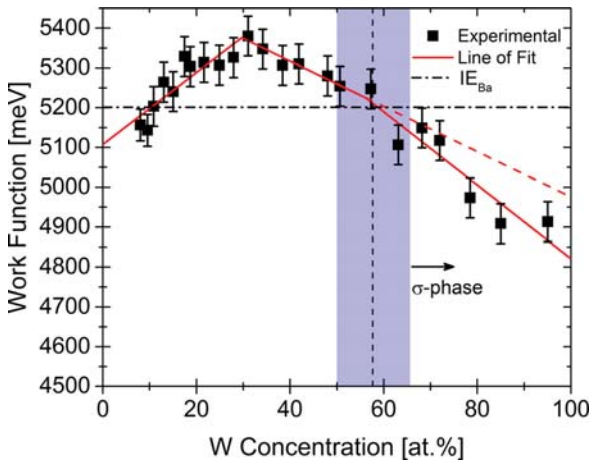

FIG. 5. (Color online) Work function and composition relationship for W–Os–Ru ternary alloys. The alloys are in the as-deposited state, with no surface or thermal treatment. The work function exhibits a peak near 30 at. % W in the W–Os–Ru alloy system and shows a sharper drop in work function at a composition corresponding to the appearance of the σ-phase. The dashed sloped line indicates the continuation of the second linear region from the piecewise fit, to show that the measured work function decreases more rapidly above 60 at. % W.

function coating will lead to enhanced electron emission from an operating cathode is supported by this result.

It is noted that the alloy thin films in this study were neither activated nor heated. As such, the grain size is lower than it would be in an active cathode coating. Nonetheless, the films studied here do represent the grain structures (phases) and orientations that have been measured in other cathode samples after activation and life testing.[16] As such, the as-sputtered films provide relevant surfaces for the measurement of alloy work function.

It is important to note the significant decrease in work function as W content increases beyond 50 at. %. The work function decreases by approximately 350 meV across the W-rich region, corresponding to a much larger difference in work function than that seen in the dilute W region. The BCT structure first appears in the alloy with 51 at. % W and is clearly evident at 63 at. % W. The appearance of the BCT phase corresponds well with the marked decrease in work function, both of which are first seen in the vertical shaded region of Fig. 5. A significant change in crystal structure should correlate with a change in work function and it appears that this is reflected in the work function trend in Fig. 5.

Work function measurements on W–Ir films of various W content revealed a similar peak in work function, occurring at slightly less than 40 at. % W. The peak is not as distinct as that observed in the W–Os–Ru alloys, but becomes clearer if one considers these values in comparison to the work functions of bulk, pure Ir and W. Figure 6 shows the measured work function trend for the W–Ir alloy films, plotted along with those of pure Ir and W from the literature.[17] The peak in alloy work function, determined from a two part piecewise linear fitting function, near 40 at. % W corresponds well with the cathode work function minimum reported by Thomas and Gibson.[8] They reported a work function minimum for B-type cathodes that had been coated with W–Ir alloy films, with the minimum occurring at approximately 40 at. % W. A three part piece-wise linear fitting function was also evaluated for fitting the data in Fig. 6, but did not fit the data as well as a two part function.

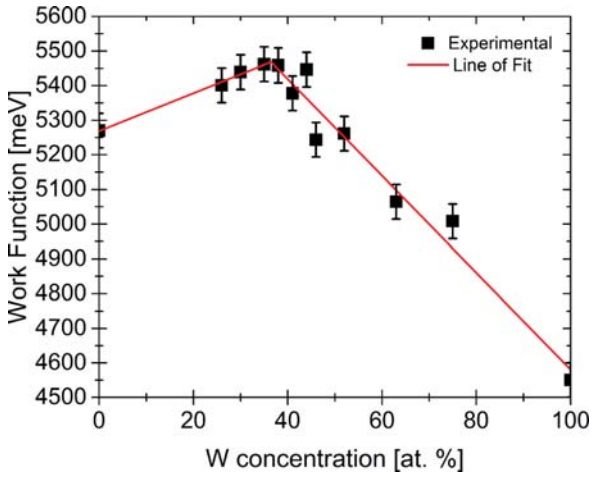

FIG. 6. (Color online) Work function trend of W–Ir alloys with respect to W concentration. There is a peak in the work function at approximately 40 at. % W. This is similar to the peak observed in the W–Os–Ru system, albeit at a slightly higher W content and with a higher value of work function.

IV. DISCUSSION

The observation that minimum values of cathode work function from emission tests correspond closely with maximum values of alloy film work function from CPD measurements supports the idea that a high work function coating will result in a cathode with a low work function, at least in certain cases. This obviously does not hold true for all coatings, as it has been shown[3,18] that high work function coatings such as gold and platinum do not produce low work function cathodes.

The question is, then, why does a high work function coating result in a low work function cathode? Zalm proposed that a coating with high work function allowed for a higher density of ionized species to adsorb on the surface. Zalm's model, however, cannot account for Au and Pt, which have high work functions yet show much poorer electron emission when coated on a B-type cathode, as compared to other platinum group metals. Skinner *et al*. have proposed a model[3] to explain the "anomalous effect," reported by Zalm, that differs from Zalm's interpretation.[1] They suggested that the differences between heats of formation for O_2 and Ba on the coatings are a better predictor of emission change than the work function of the coating alone.[3] Their model also accounts for Au and Pt, making it more robust than Zalm's. Looking strictly at the cathode work function (i.e., not the work function of the coating, but the work function determined during emission testing), Thomas and Gibson asserted that there are both compositional and structural reasons for their observed work function minima.[8] They postulate that composition influences the direction of the charge transfer between the adsorbed Ba/O and the coating. They also suggest that the surface configuration of the alloys in their study could explain why some minima occur at slightly different concentrations of W.

From the results of this study, it is unclear why the W–Os–Ru ternary alloy system would exhibit a maximum in work function at 30 at. % W. Only the HCP structure was detected for alloys in this composition range where the peak was observed. The existence of the σ-phase was detected only at higher W concentrations (above 60 at. % W) and corresponded to the onset of a steep decrease in work function. Furthermore, there was no disproportionate variation in lattice parameters in the HCP phase near 30 at. % W, where the work function maximum occurred. The films' textures, determined from relative peak intensities measured from the XRD scans, were analyzed in order to evaluate whether texture could account for the work function trend. However, the trend in film textures could not describe the observed changes in WF. While the work functions of individual crystallographic facets are unknown in this alloy system, work function generally increases with planar atomic density. Therefore, the {0002} orientation should have the highest work function, followed by the {10–10} and {10–11}

orientations. The relative intensity of the {0002} texture component has a maximum value near 20 at. % W, and is approximately the same at 0 and 40 at. % W. However, this does not coincide with the WF trend and it is unlikely that the trend in work function near 30 at. % W is due solely to crystallographic effects.

However, it is possible that the complex nature of the bonding between W, Os, and Ru could explain the work function maximum by considering modifications to the molecular orbitals and Fermi level. A composition of 30 at. % W may represent the optimum modification of the oxidation state of the alloy, resulting in the lowest Fermi level and therefore the highest work function. Modification of the electronic structure of the alloy may be the most reasonable interpretation of results, albeit somewhat speculative, in view of the following discussion.

Greiner *et al*. have described energy-level alignment in transition metal oxides[19] that may shed light on why a high work function coating leads to enhanced electron emission. They show that the charge transfer between an adsorbed species and the metal oxide is most efficient when the work function of the substrate (metal oxide) is greater than the ionization energy of the adsorbed species. The current understanding of Ba at the cathode surface is that it exists in metallic form[3,5,20] as an adsorbed monolayer above O, which in turn sits atop the alloy substrate.[2] The alloy surface forms very early and may even form during the initial heating stages that activate the cathode.[21] The charge transfer from Ba to O or to the substrate results in an electric dipole that allows for a lowering of the potential energy barrier to thermionic emission. Considering this, the oxidized substrate work function should be greater than the ionization energy of Ba (IE_{Ba}) for the greatest charge transfer to the substrate. Given that the first ionization energy of Ba is approximately 5.2 eV, and assuming that the theory described by Greiner *et al*. is valid, it follows that for the greatest charge transfer, the substrate should have a work function of 5.2 eV or greater.

According to the experimental results shown in this study, the work function of W–Os–Ru is close to 5.2 eV at low W concentrations. For increasing concentrations of W in the W–Os–Ru alloy films, the work function increases to almost 5.4 eV at approximately 30 at. % W, and then decreases to 5.2 eV at approximately 60 at. % W. Therefore, W–Os–Ru alloys at concentrations less than 60 at. % W should allow for efficient charge transfer from Ba, yielding an enhanced electric dipole and, therefore, enhanced thermionic emission. Furthermore, the greatest charge transfer should occur at approximately 30 at. % W, where the highest work function is observed. At 60 at. % W, the W–Os–Ru alloy was observed to transform into the σ-phase, after which a more rapid decline in work function with rising W concentration was also observed. Implicit to this line of reasoning is that the work functions were measured for alloys with a surface oxide, since the theory of Greiner *et al*.[19] is based on transition metal oxide surfaces. The alloys in the current study were expected to have some surface oxide layer because they were exposed to atmospheric conditions between deposition and measurement of the work function. This was confirmed by XPS, which showed that all alloys exhibited an oxide layer. Figure 7 presents the surface chemistry for a typical W–Os–Ru alloy film.

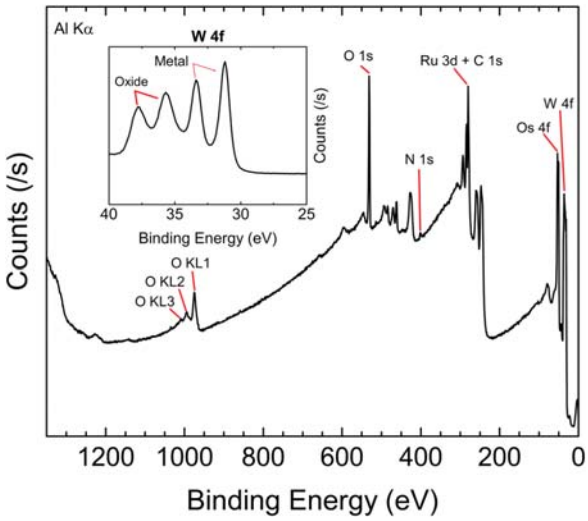

FIG. 7. (Color online) XPS spectrum of W–Os–Ru (51 at. % W) in the as-deposited state. The inset region for W 4f peaks indicates that the alloy surface is partially oxidized. All peaks for major species are labeled. Other peaks can be attributed to core levels of W, Os, or Ru. Additional W–Os–Ru alloy compositions yielded similar spectra.

These results mesh well the theory of Greiner *et al*.[19] when coupled with experimental thermionic emission data from Thomas and Gibson.[8] The cathode work function minima at approximately 40 at. % W for W–Os and W–Ir (Ref. 8) can be attributed to the work function maxima for the respective alloy coatings, which allow for the greatest Ba charge transfer to the substrate. Furthermore, the observed decline in electron emission for alloy films with increasing amounts of the σ-phase can be explained by a reduction in the alloy coating work function below 5.2 eV, the ionization energy of Ba. Coatings with work functions below 5.2 eV would not allow for efficient charge transfer from Ba to the substrate, resulting in a weakening of the electric dipole and a decrease in thermionic emission. Applying the theory of Greiner *et al*. to dispenser cathodes is compelling in that it accounts for improved electron emission from a high work function coating as well as the outliers of Au and Pt, because Au and Pt do not readily form oxides.

V. SUMMARY AND CONCLUSIONS

W–Os–Ru ternary alloy films were sputter deposited with a gradient in W concentration and their crystal structure and work function were characterized. The goal was to explore relationships between film microstructure, work function, and thermionic emission. While the alloy thin films in this study were not heated nor impregnated, they did exhibit both HCP and BCT phases, and thus represent the crystal structures that are experimentally observed in activated and tested cathode surface coatings. The correlation of measured work function peaks in the as-deposited gradient films with emission maxima found in the CSD testing of Os–Ru and Ir

coated cathodes as reported by Thomas and Gibson[8] reinforces the comparisons drawn in this study. It was shown that the work function values of W–Os–Ru alloys decrease from ~5.4 eV as the W concentration deviates from 30 at. % W (i.e., there is a maximum at 30 at. %). Additionally, the rate of decrease with W concentration is steeper beyond 60 at. % W, which corresponds to the onset of the BCT σ-phase in the sputtered W–Os–Ru films. The work function maximum at 30 at. % W for as-deposited W–Os–Ru is correlated with a work function minimum (as calculated from thermionic emission data) observed for dispenser cathodes with an alloy coating of composition 40 at.% W–60 at. % Os. Similarly, as-deposited W–Ir films exhibited a work function maximum near 40 at. % W, which corresponds to the work function minimum observed for dispenser cathodes coated with a 40 at. % W–60 at. % Ir alloy film.

These results are consistent when considered in light of the work on energy-level alignment of molecules on metal oxides by Greiner *et al*. Accordingly, as the work function of the substrate increases beyond the ionization energy of the adsorbed material, the resultant charge transfer from the adsorbent to the substrate becomes more efficient. If the first ionization level of Ba is taken to be 5.2 eV, it is not surprising that a cathode coated with an alloy film having a maximum work function of ~5.4 eV in the as-deposited state would yield the lowest work function cathode. It is also not surprising that thermionic emission decreases more rapidly (with higher concentrations of W) as the σ-phase becomes a more prominent constituent in the coating, as this phase has a work function less than 5.2 eV.

Interestingly, one implication from this study is that a cathode coated with a W–Ir alloy film should yield a lower work function than a W–Os–Ru alloy coated cathode, as the W–Ir alloy work function maximum (~5.45 eV) is higher than that for W–Os–Ru (~5.38 eV). Disagreement over which coating (Ir or Os–Ru) results in better electron emission could simply stem from the composition of the alloy coating when the emission data were collected. Additionally, the Kelvin probe may prove to be a valuable technique to evaluate dispenser cathode coatings without relying solely on extensive high temperature experiments.

ACKNOWLEDGMENTS

This material was based upon work supported by the National Science Foundation under Grant No. CMMI-0928845. Use of the XPS was supported by the National Science Foundation under Grant No. 0814194.

[1]P. Zalm and A. J. A. Van Stratum, Philips Tech. Rev. **27**, 69 (1966).
[2]R. Cortenraad, A. W. D. van der Gon, H. H. Brongersma, G. Gärtner, and A. Manenschijn, Appl. Surf. Sci. **191**, 153 (2002).
[3]H. B. Skinner, R. A. Tuck, and P. J. Dobson, J. Phys. D: Appl. Phys. **15**, 1519 (1982).
[4]M. C. Green, H. B. Skinner, and R. A. Tuck, Appl. Surf. Sci. **8**, 13 (1981).
[5]J. L. Cronin, IEE Proc.-I **128**, 19 (1981).
[6]D. Jones, D. McNeely, and L. W. Swanson, Appl. Surf. Sci. **2**, 232 (1979).
[7]A. J. A. van Stratum, J. Appl. Phys. **42**, 4436 (1971).
[8]R. E. Thomas and J. W. Gibson, Appl. Surf. Sci. **29**, 49 (1987).
[9]D. Brion, J. C. Tonnerre, and A. Shroff, Appl. Surf. Sci. **20**, 429 (1985).
[10]A. Shih, A. Berry, C. R. K. Marrian, and G. A. Haas, IEEE Trans. Electron Devices **34**, 1193 (1987).
[11]H. Baker and H. Okamoto, *Introduction to Alloy Phase Diagrams* (ASM International, OH, 1992).
[12]D. Brion, J. C. Tonnerre, and A. M. Shroff, Appl. Surf. Sci. **16**, 55 (1983).
[13]L. R. Falce, Int. Electron. Devices Meet. **29**, 448 (1983).
[14]M. F. Koenig and J. T. Grant, Appl. Surf. Sci. **20**, 481 (1985).
[15]N. J. A. Vanveen, Appl. Surf. Sci. **29**, 113 (1987).
[16]P. D. Swartzentruber, T. J. Balk, and M. P. Effgen, J. Vac. Sci. Technol., A **32**, 040601 (2014).
[17]H. B. Michaelson, J. Appl. Phys. **48**, 4729 (1977).
[18]R. A. Tuck, Platinum Met. Rev. **26**, 167 (1982).
[19]M. T. Greiner, M. G. Helander, W. M. Tang, Z. B. Wang, J. Qiu, and Z. H. Lu, Nat. Mater. **11**, 76 (2012).
[20]D. S. Chen, I. Lindau, M. H. Hecht, A. J. Viescas, J. Nogami, and W. E. Spicer, Appl. Surf. Sci. **13**, 321 (1982).
[21]K. D. Rachocki, B. C. Lamartine, and T. W. Haas, Appl. Surf. Sci. **16**, 40 (1983).